Dysregulated Arginine Metabolism Is Linked to Retinal Degeneration in *Cep250* Knockout Mice

Lue Xiang,[2] Qiao-Li Yang,[2] Bin-Tao Xie,[2] Hui-Yi Zeng,[2] Liu-Jun Ding,[2] Feng-Qin Rao,[2,3] Tong Yan,[2] Fan Lu,[2] Qi Chen,[2] and Xiu-Feng Huang[1]

[1]Zhejiang Provincial Clinical Research Center for Pediatric Disease, The Second Affiliated Hospital and Yuying Children's Hospital of Wenzhou Medical University, Wenzhou, Zhejiang, China
[2]State Key Laboratory of Ophthalmology, Optometry and Visual Science, Eye Hospital, Wenzhou Medical University, Wenzhou, Zhejiang, China
[3]School of Pharmaceutical Sciences of Wenzhou Medical University, Wenzhou, Zhejiang, China

Correspondence: Xiu-Feng Huang, Zhejiang Provincial Clinical Research Center for Pediatric Disease, The Second Affiliated Hospital and Yuying Children's Hospital of Wenzhou Medical University, Wenzhou, Zhejiang, China; hxfwzmc@163.com.
Qi Chen, State Key Laboratory of Ophthalmology, Optometry and Visual Science, Eye Hospital, Wenzhou Medical University, Wenzhou, Zhejiang, China; qichen1983@eye.ac.cn.
Fan Lu, State Key Laboratory of Ophthalmology, Optometry and Visual Science, Eye Hospital, Wenzhou Medical University, Wenzhou, Zhejiang, China; lufan62@mail.eye.ac.cn.

LX, QLY, and BTX contributed equally to this work.

Received: March 6, 2023
Accepted: August 4, 2023
Published: September 1, 2023

Citation: Xiang L, Yang QL, Xie BT, et al. Dysregulated arginine metabolism is linked to retinal degeneration in *Cep250* knockout mice. *Invest Ophthalmol Vis Sci.* 2023;64(12):2. https://doi.org/10.1167/iovs.64.12.2

Purpose. Degeneration of retinal photoreceptors is frequently observed in diverse ciliopathy disorders, and photoreceptor cilium gates the molecular trafficking between the inner and the outer segment (OS). This study aims to generate a homozygous global Cep250 knockout (KO) mouse and study the resulting phenotype.

Methods. We used *Cep250* KO mice and untargeted metabolomics to uncover potential mechanisms underlying retinal degeneration. Long-term follow-up studies using optical coherence tomography (OCT) and electroretinography (ERG) were performed.

Results. OCT and ERG results demonstrated gradual thinning of the outer nuclear layer (ONL) and progressive attenuation of the scotopic ERG responses in *Cep250*$^{-/-}$ mice. More TUNEL signal was observed in the ONL of these mice. Immunostaining of selected OS proteins revealed mislocalization of these proteins in the ONL of *Cep250*$^{-/-}$ mice. Interestingly, untargeted metabolomics analysis revealed arginine-related metabolic pathways were altered and enriched in *Cep250*$^{-/-}$ mice. Mis-localization of a key protein in the arginine metabolism pathway, arginase 1 (ARG1), in the ONL of KO mice further supports this model. Moreover, adeno-associated virus (AAV)-based retinal knockdown of Arg1 led to similar architectural and functional alterations in wild-type retinas.

Conclusions. Altogether, these results suggest that dysregulated arginine metabolism contributes to retinal degeneration in *Cep250*$^{-/-}$ mice. Our findings provide novel insights that increase understanding of retinal degeneration in ciliopathy disorders.

Keywords: arginase 1, arginine, photoreceptors, ciliopathy disorders; *Cep250*

Ciliopathy disorders encompass a broad range of clinical manifestations caused by genetic defects in cilia-related genes.[1,2] Because retinal photoreceptors have specialized primary cilia structures, degeneration of retinal photoreceptors is frequently observed in diverse ciliopathy disorders.[1] The photoreceptor connecting cilium elaborates into outer segment discs, which are responsible for photon capture and visual transduction. In addition, photoreceptor cilium gates the molecular trafficking between the inner and the outer segment (OS). Interestingly, although some cilia-related proteins are distributed across different ciliary structures, their mutations often give rise to common retinal phenotypic changes.[3] Multiple studies have demonstrated that mutant mice of cilia-related genes display attenuated electroretinography (ERG) responses and progressive apoptosis of photoreceptor cells.[3–6] More importantly, the depletion of ARL13B, INPP5E, CEP290, NPHP5, and TMEM138 in mice resulted in changes similar to the distribution of some outer segment proteins, including RHO, M-OPSIN, S-OPSIN, PDE6B, RPHP2, PROM1.[7–11] Despite extensive studies, many gaps remain in the mechanism of protein trafficking across the photoreceptor cilium. Do these mislocalized OS proteins trigger retinal degeneration, or is their mislocalization caused by some uncharacterized pathogenic mechanism?

Photoreceptor cells have high energy and amino acid metabolism requirements.[12–17] A large number of studies have found that insufficient energy supply and disordered lipid and amino acid metabolism are often closely related to the occurrence and progress of retinal diseases and thus may potentially act as driving factors promoting retinal degeneration.[12–17] A recent study identified a BBS1 mutation affecting not only OS proteins but also OS lipid composition, leading to the suggestion that progressive morphological defects could be explained by disruption of OS lipid homeostasis.[18] Another study reported that the neuroprotective gene CNTF protects against retinal degradation by significantly impacting the metabolic status of aerobic glycolysis and augmenting anabolic activities. These clues have led us to pay more attention to metabolic status in retinal degeneration.[19]

Notably, metabolomics offers an opportunity to analyze an organism's endogenous metabolites, which is the most recently developed "omics" in the area of system biology. The metabolites are the downstream of the genetic transcription and translation processes, which thereby are thought to relate closely to the phenotype. Recently, there has been increasing interest and research in the metabolomics of ocular diseases. The application of metabolomics to retinal diseases, with a focus on age-related macular degeneration,[20] diabetic retinopathy,[21] retinopathy of prematurity,[22] and retinitis pigmentosa,[23] has proven that metabolomic profiling is a promising tool for discovering biomarkers that improve our understanding of the pathogenesis of retinal disease.[24,25] In this study, we used Cep250 knockout (KO) mice and untargeted metabolomics to uncover a potentially novel pathogenic mechanism underlying retinal degeneration in ciliopathy disorders.

Methods

Generation of *Cep250* Knockout Mice

Cep250 KO mice were generated in a C57BL/6J background using the CRISPR/Cas9 system. The mouse Cep250 gene (ENSMUSG00000038241) is located on chromosome 2 (Supplementary Fig. S1A). The sgRNAs targeting intron 2 and intron12 were used in this study. Ultimately, exon 3 to exon 12 were removed from the Cep250 gene in KO mice. Founders were genotyped by DNA sequencing and T7E1 analysis. Genotyping primers, design strategy and example genotyping results are shown in Supplementary Figures S1B and S1 C.

Animal Care and Use

All mice were raised in the mouse facility of the School of Ophthalmology and Optometry at Wenzhou Medical University and were authorized by the Institutional Animal Care and Use Committee of Wenzhou Medical University.[26,27] The experiments in this study were carried out according to the Association for Research on Vision and Ophthalmology's statement.

Fundus Photography

To survey potential fundus defects in Cep250 KO mice, fundus photography (FP) was performed using a Micron IV retinal imaging system (Phoenix Research Laboratories, Pleasanton, CA, USA). To dilate the pupils of each mouse eye, 0.5% tropicamide was applied for five minutes. Mice were then anesthetized intraperitoneally with a liquid mixture of ketamine (80 mg/kg) and xylazine (16 mg/kg). Dicolol (ofloxacin eye ointment) was daubed onto the cornea to keep it moist. After calming down, experimental mice were faced toward the MICRON IV camera to obtain FP images.

Immunostaining and TUNEL Staining

The eyeballs of experimental mice were excised from euthanized mice as quickly as possible and fixed in 4% paraformaldehyde for about 15 minutes. After removal of the cornea and lens, the eyecups were refixed in 4% paraformaldehyde for an additional 20 min. Subsequently, the eyecups were dehydrated three times in 30% sucrose (wt/vol) in PBS and, finally, embedded in embedding medium (Neg-50, Thermo). In the present study, 18 µm retinal cryosection slides were prepared, and samples were rinsed three times in 0.01 M PBS. Targeted retinal tissues were blocked in blocking buffer (composed of 4% bovine serum albumin and 0.5% Triton X-100) for two hours at room temperature. For immunostaining experiments, slides were incubated with primary antibodies at 4°C overnight. Subsequently, diluted secondary antibodies were added to the tissues at room temperature for one hour. The primary antibodies and dilutions used in this study were as follows: rabbit-anti-Arg1 (1: 200; Abcam, Cambridge, MA, USA); mouse-anti-Arg2 (1:200; Santa Cruz Biotechnology, Dallas, TX, USA); rat-anti-GFAP (1:500; Millipore, Burlington, MA, USA); rabbit-anti-Opn1sw (1:200; Millipore); rabbit-anti-Rhodopsin (1: 1000; Sigma-Aldrich Corp., St. Louis, MO, USA); and rabbit-anti-Opn1mw (1:200; Millipore). The secondary antibodies used in this study were donkey anti-rabbit Alexa488 (1:200; Jackson Laboratories, Bar Harbor, ME, USA), donkey anti-rabbit Alexa647 (1:200; Jackson Laboratories), donkey anti-mouse Alexa594 (1:200; Jackson Laboratories), and donkey anti-rat Alexa488 (1:200; Jackson Laboratories). A 4′,6-diamidino-2-phenylindole (DAPI, 1:5000; Sigma-Aldrich Corp.) was used to stain the cell nuclei of targeted tissues. TUNEL in situ labeling was performed using the One Step TUNEL Apoptosis Assay Kit (Beyotime Institute of Biotechnology, Jiangsu, China) based on the manufacturer's protocol 25. Ultimately, images of immunostained samples were obtained using a ZEISS confocal microscope (LSM880; Zeiss, Oberkochen, Germany).

ERG

Cep250 KO and age-matched control mice were paired for the RETI-port ERG system (Ganzfeld Q450 SC; Roland Consult, Brandenburg, Germany), and experiments were conducted as previously described.[28] In this study, these experiments were carried out in the afternoon. For dark-adaption, experimental mice were kept in the dark room for more than two hours and then anesthetized with a mixture of ketamine (100 mg/kg) and xylazine (10 mg/kg). Mouse pupils were dilated by tropicamide, and gold wire loop electrodes were carefully touched to both corneas of each mouse. During the experiment, mice were placed on a heating pad to maintain their body temperatures at about 37°C. ERG was conducted based on the protocol previously described.[28] The parameters of stimulation intensities for photopic responses were as follows: 0.20, 0.63, 2, 6.3, and 20 cd/m^2. The parameters for scotopic responses were as follows: 0.0002, 0.0063, 0.20, 2, and 6.3 cd/m^2.

Retinal Isolation and Metabolic Profiling

Retinas from both eyes of wild-type (WT) and Cep250 KO mice were used for metabonomic analysis. The retinas were rapidly isolated from the eyecups and were immediately frozen in liquid nitrogen. Retinal samples were homogenized at 50 Hz × 4°C for three minutes in 300 µL ice-cold extraction solution (acetonitrile/methanol/H_2O = 2:2:1, with 0.5 µg/mL L-chlorophenylalanine used as an internal standard). Proteins were pelleted by centrifugation, and 250 µL supernatant was collected. Metabolites were dried in a vacuum centrifuge and resuspended in 10% methanol. A quality control (QC) sample was prepared by mixing equal amounts of the extracted samples.

LC-MS/MS analysis was performed with an Ultimate 3000 UHPLC system combined with Orbitrap Fusion Lumos mass spectrometer (Thermo Fisher Scientific, Waltham, MA, USA). Chromatographic separation was performed using an Acquity HSS T3 column (Waters Corporation, Milford, MA, USA) (1.8 µm × 2.1 mm × 100 mm) with a 20 min gradient. The flow rate was 0.3 mL/min, and the column temperature was 35°C. In positive ion mode, mobile phase A was H_2O with 0.1% formic acid, and mobile phase B was methanol with 0.1% formic acid. In negative ion mode, mobile phase A was 6.5 mM NH_4HCO_3 solution, and mobile phase B was methanol.

The mass spectrometer was operated under electrospray ionization positive and negative modes. The full scan (m/z 70–1050) was performed with a resolution of 120,000, automatic gain control target of 4×10^5 ions, and maximum ion injection time of 50 ms. Data-dependent MS/MS data were acquired on the top speed mode with a cycle time of 0.8 second and the following settings: resolution: 30,000, automatic gain control: 5×10^4 ions, maximum injection time: 54 ms, stepped high-energy collisional dissociation (HCD) normalized collision energy: 15%, 30%, and 50%.

Untargeted Metabolomics Data Analysis

Raw data were analyzed by Compound Discoverer 3.3 (Thermo Fisher Scientific) in both positive and negative ion modes. Unknown compounds were detected and grouped with a 5 ppm mass tolerance. MS/MS spectra were searched using the mzCloud library. Metabolites with area relative standard deviations (RSDs) greater than 30% in the QC samples were filtered. *P* values were calculated by the two-tailed Student's *t* test. Metabolites with *P* values < 0.05 were selected as differentially expressed metabolites. Principal component analysis was conducted using SIMCA 14.1. Identified metabolites were mapped to Kyoto Encyclopedia of Genes and Genomes (KEGG) pathways and assessed for enrichment using MetaboAnalyst 5.0.

AAV2/9-Mediated Arg1 Knockdown Experiments

A knockdown adeno-associated virus for Arg1 was prepared by Shanghai Genechem Co., Ltd. (Shanghai, China). To generate AAV2-mmu-Arg1 RNAi, the target sequence "GCCGATTCACCTGAGCTTTGA" was cloned into a GV478 vector containing U6-MCS-CAG-EGFP. The AAV2-mediated empty vector containing U6-MCS-CAG-EGFP was used as a control. The titer of AAV2-mmu-Arg1 RNAi was 1.05×10^{12} TU/mL. Adeno-associated virus (AAV) solution 1 µL was injected into the subretinal space of each mouse eye using a blunt Hamilton syringe held in a 5-µL micromanipulator.

Optical Coherence Tomography Image Acquisition and Analysis

Optical coherence tomography (OCT) experiments were performed as previously described.[28] High-resolution spectral-domain OCT (Spectralis HRA + OCT; Heidelberg Engineering, Heidelberg, Germany) was usesd to obtain intraretinal layer images of experimental mice in the horizontal meridian centered on the optic nerve head. To prepare the mice for OCT experiments, their pupils were dilated, and the mice were anesthetized as in ERG experiments. Dicolol was administered to the corneas to keep them moist. Subsequently, experimental mice were positioned on the experimental platform for image acquisition. The boundaries of the intraretinal layers were defined manually using the commercially available ImageJ software program (version 1.53, National Institutes of Health, Bethesda, MD, USA). Thicknesses of the whole retina and intraretinal layers (outer nuclear layer [ONL] and IS/OS layer) were then calculated using MATLAB software (Mathworks Inc., Natick, MA, USA).

Arginine Quantification by LC-MS/MS

Arginine extraction was performed following the procedure described previously. [29] Briefly, retina samples were obtained from mice injected with AAV at P30 and collected at P90. The retinas were homogenized in 150 µL of ddH2O and then spun in a centrifuge at 16,000 rpm for 10 minutes. The resulting supernatant was transferred to a new tube and deproteinized by adding 200 µL of methanol. After vigorous vortexing, the sample was spun in a centrifuge at 16,000 rpm and 4°C for 10 minutes. Subsequently, the supernatant was transferred to a sample vial for LC-MS/MS analysis. The arginine standards underwent the same treatment as the retina samples to prepare the calibration curve. LC-MS/MS analysis was performed using a Thermo Fisher Ultimate 3000 liquid chromatography system (Thermo Fisher Scientific) coupled with an Orbitrap Fusion Lumos mass spectrometer (Thermo Fisher Scientific). Chromatographic separation was conducted using a flow rate of 0.6 mL/min and using a Synchronis HILIC column (1.7 µm, 2.1 × 100 mm). The separation utilized a gradient elution with mobile phase A (H_2O containing 0.1% formic acid and 20 mM ammonium formate) and mobile phase B (90% acetonitrile containing 0.1% formic acid and 20 mM ammonium formate). The gradient used was as follows: 0 to 0.5 minute with 95% solvent B, 0.5 to 3.0 minutes with 80% solvent B, 3.0 to 4.0 minutes with 60% solvent B, 4.0 to 4.1 minutes with 95% solvent B, and 4.1 to 5.5 minutes with 95% solvent B. Ionization of the samples was performed using an H- electrospray ionization source, and the mass spectrometer was operated in positive ion mode. Mass spectra were acquired using the PRM mode, which included full MS1 scans and targeted MS2 scans of the parent ion with m/z 175.11895.

Statistical Analyses

The data are shown as mean ± SEM, and statistical significance was analyzed using the two-tailed Student's *t* test. The results were visualized using GraphPad Prism. **P* < 0.05, ***P* < 0.01, and ****P* < 0.001 between the KO and WT control groups.

Results

Cep250 Deficiency Leads to Retinal Morphological Alterations

To directly assess the retinal structure in vivo, spectral-domain OCT and fundus color photography were used to screen the retinal morphologies of *Cep250*$^{-/-}$ mice at postnatal days (P) 30, P90, P180, and P270. Notably, OCT images revealed significant morphological alterations in *Cep250*$^{-/-}$ mice at each evaluation time point (Fig. 1). Based on analysis of ONL thickness, the photoreceptor layer was significantly thinned in *Cep250*$^{-/-}$ mice at P30, P90, P180, and P270 (Figs. 1A, 1B). Significant thickness changes to the combined inner segment and outer segment layers (IS/OS) were also observed between these two groups (Fig. 1C). Consistently, differences in the ONL and IS/OS between WT and *Cep250*$^{-/-}$ mice were reflected in differences in whole-retina thickness (Fig. 1D). We also performed fundus photography (FP) to examine the retinal morphologies of *Cep250*$^{-/-}$ mice from P30 to P270. Of note, fundus images revealed a blurry atrophic macular area, nummular pigmentation and attenuation of retinal blood vessels during aging in *Cep250*$^{-/-}$ mice (Supplementary Fig. S2). These results demonstrate that *Cep250*$^{-/-}$ mice suffer from progressive retinal morphological alterations.

Cep250 Deficiency Results in Retinal Functional Impairment

To further investigate the functional changes in *Cep250*$^{-/-}$ mice, we recorded ERG responses at P30, P90, P180, and P270 (Fig. 2A). At the inspected time points during aging, we observed significant differences in scotopic responses (Dark 3.0 and Dark 10.0), while the photopic responses (Light 3.0) exhibited lower a-waves and b-waves but without significant differences between WT and the *Cep250*$^{-/-}$ mice (Figs. 2B–E, Supplementary Figs. S3A–D). The amplitudes of retinal scotopic responses gradually decreased during aging in *Cep250*$^{-/-}$ mice and were significantly lower than those in WT mice at all time points examined (Figs. 2B–E, Supplementary Figs. S3A–D). Notably, *Cep250*$^{-/-}$ mice exhibited a nominal effect on photopic ERG responses until the final time point (P270) (Fig. 2E, Supplementary Fig. S3D). Altogether, the results of ERG experiments demonstrate that *Cep250* deficiency can result in progressive impairment of retinal functions.

Cep250 Deficiency Affects OS-Protein Localization

Subsequently, we assessed cilia function during retinal development by immunostaining the retinas of *Cep250*$^{-/-}$ mice at P15 and P30 using antibodies against OS proteins,

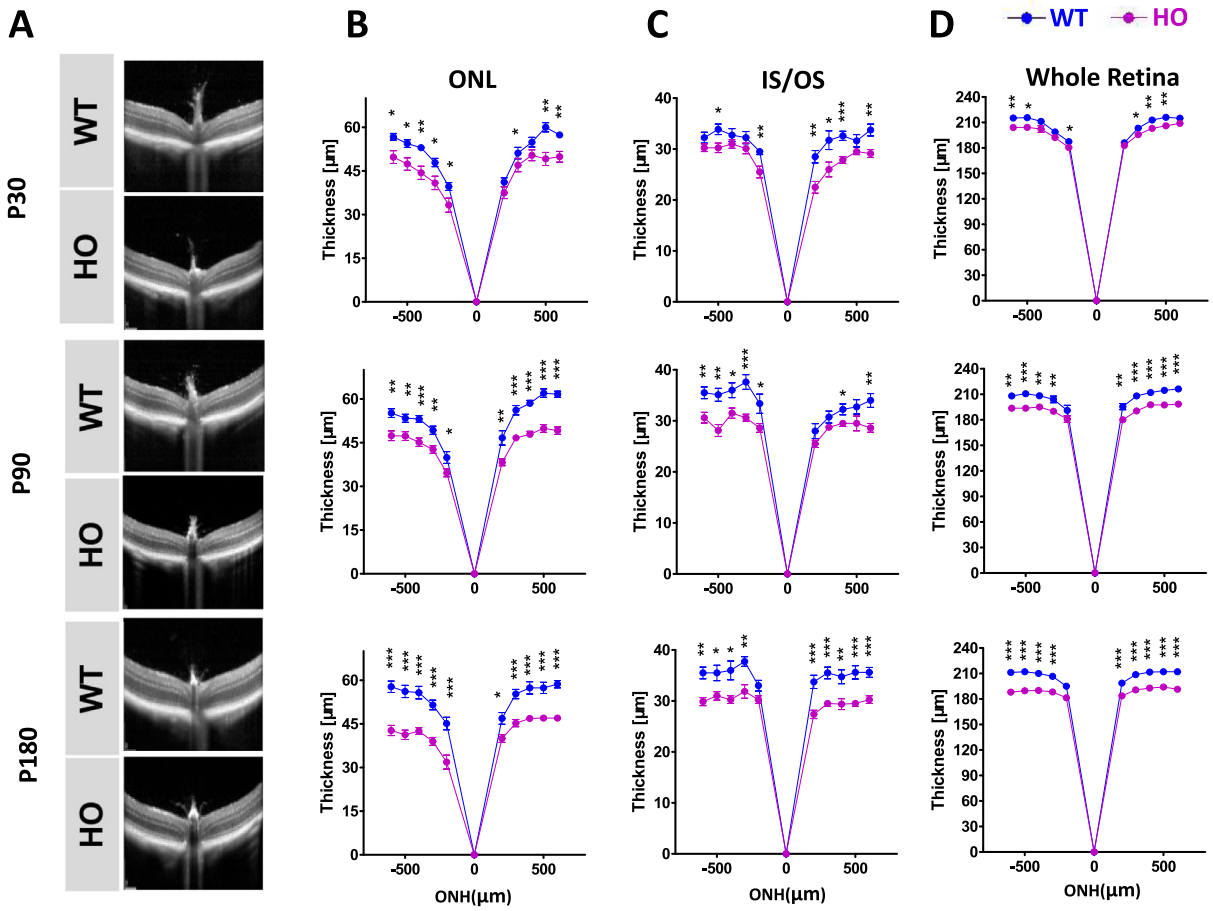

Figure 1. Segmentation of the retinal layers in WT and Cep250 KO mice. (**A**) Representative images of WT and Cep250 KO mice along with nasal and temporal orientation. *Scale bars*: 100 μm. WT, Wild-types; HO, Homozygotes. (**B–D**) Measurements of the thicknesses of the ONL (**B**), OS/IS (**C**), and the whole retina (**D**) from OCT images of mice at P30, P90 and P180. ONH, optic nerve head. Normalized values represent mean ± SEM.*$P < 0.05$, **$P < 0.01$, and ***$P < 0.001$, Student's t test. n = 6.

Investigative Ophthalmology & Visual Science

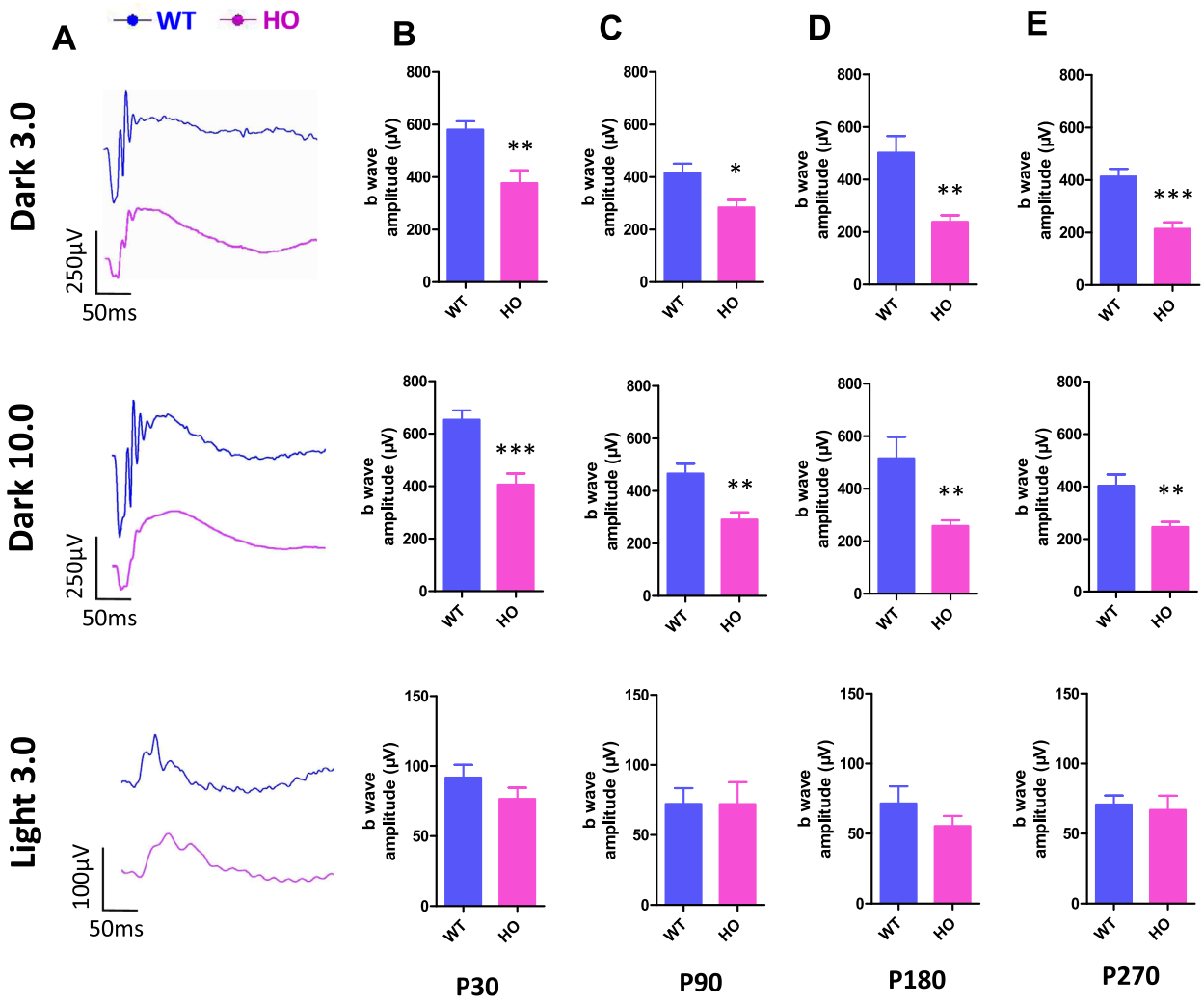

Figure 2. Evaluation of retinal function in Cep250 KO mice. (**A**) Representative ERG waves at dark 3.0, dark 10.0 and light 3.0. (**B–E**) Statistical analysis of b-wave amplitudes at dark 3.0, dark 10.0 and light 3.0. Experimental time points were P30 (**B**), P90 (**C**), P180 (**D**) and P270 (*E*). n = 8. *Error bars* represent SEM. **P* < 0.05, ***P* < 0.01, and ****P* < 0.001. HO, Homozygotes.

including rhodopsin, M-opsin, and S-opsin. Our data revealed that a small proportion of RHODOPSIN proteins were mislocalized in the ONL of *Cep250*$^{-/-}$ mice at P15 and P30, with this pattern not observed in WT mice (Fig. 3A). A similar defect was exhibited in M-opsin immunostaining of *Cep250*$^{-/-}$ mice at P15 and P30 (Fig. 3B). S-opsin protein localization was also changed in homozygous KO mice at P30, although not at P15 (Fig. 3C). In addition, results from TUNEL assays revealed increased cell death in *Cep250*$^{-/-}$ mice compared to WT mice (Fig. 3D). Together, these data indicate a progressive loss of photoreceptor cells.

Untargeted Metabolomics Analysis of *Cep250*$^{-/-}$ Mouse Retinas

To address whether dysfunction in Cep250 gives rise to retinal degeneration through a metabolic pathway, we carried out untargeted metabolomics analysis of P30 and P90 mouse retinas. Principal component analysis indicated good repeatability for both positive and negative ion modes (Supplementary Fig. S4A, S4B). The QC samples were clustered closely together, suggesting good sample quality (Supplementary Fig. S4A). Significant alternations in metabolites were identified using the criteria of fold change > 1 and $P < 0.05$. Metabolomic differences between the two groups were visualized using Volcano plots (Supplementary Fig. S4C). At P30, we identified 100 differentially expressed metabolites under negative ion mode in *Cep250*$^{-/-}$ mice compared with WT mice, including 67 upregulated metabolites and 33 downregulated metabolites. Under positive ion mode, we identified a total of 118 differentially expressed metabolites, including 64 upregulated and 54 downregulated metabolites. At P90, we identified 52 differentially expressed metabolites in *Cep250*$^{-/-}$ mice compared to WT mice using negative ion mode. Among these metabolites, 13 were upregulated and 39 were downregulated. Under positive ion mode, we detected a total of 177 differentially expressed metabolites, consisting of 58 upregulated and 119 downregulated metabolites.

Investigative Ophthalmology & Visual Science

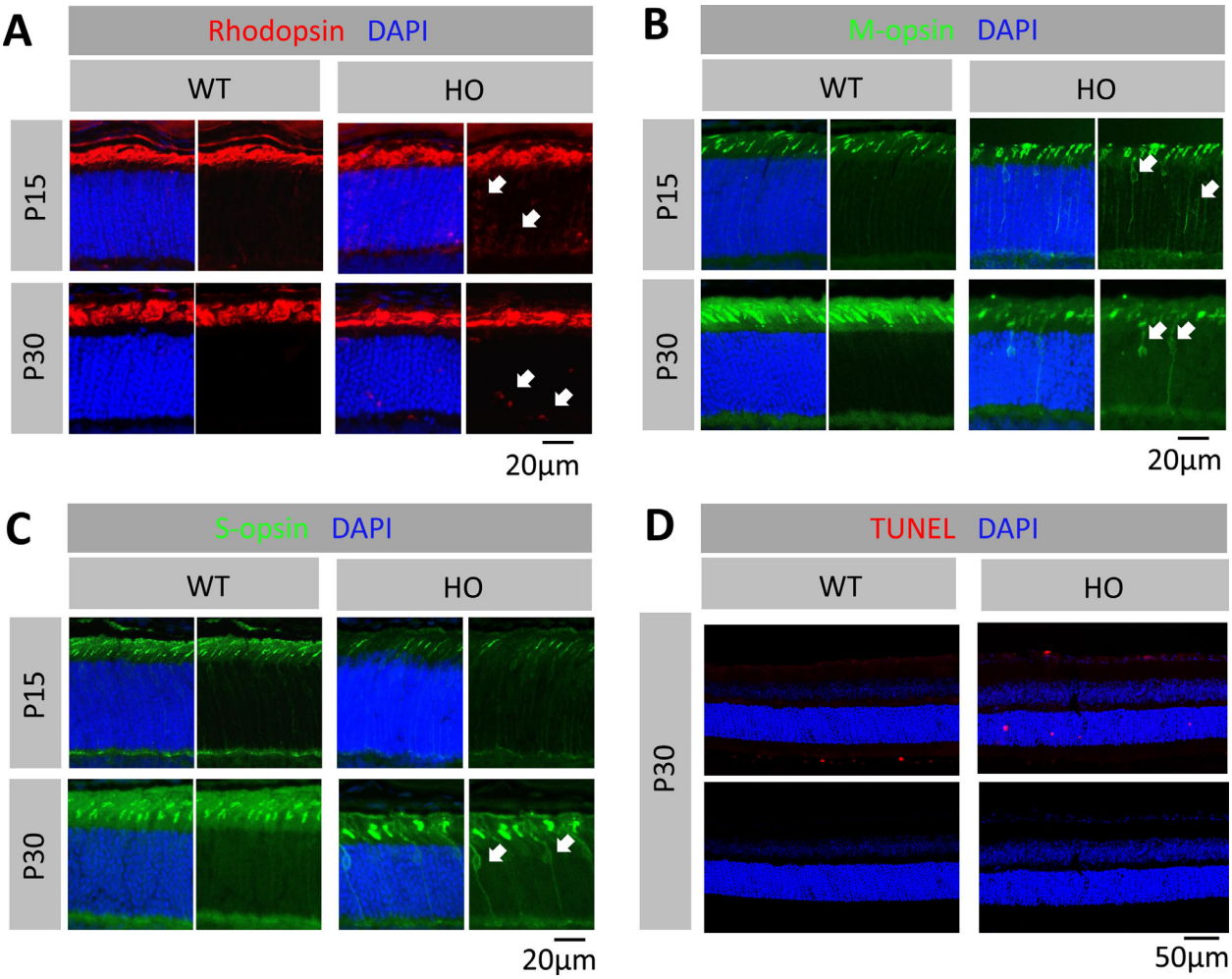

Figure 3. TUNEL staining and immunostaining of Rhodopsin, M-opsin and S-opsin in WT and Cep250 KO mouse retinas. (**A–C**) Representative images of Rhodopsin (**A**), M-opsin (**B**), and S-opsin (**C**) immunostaining results in WT (*left*) and HO (*right*) mouse retinas. *White arrows* indicate the dislocation of photosensitive proteins in the ONL. *Scale bar*: 20 μm. (**D**) Representative images of TUNEL staining results in WT (*left*) and HO (*right*) mouse retinas. n = 3. *Scale bar*: 50 μm. HO, Homozygotes.

Metabolomic Signatures in the Retinas of *Cep250*$^{-/-}$ Mice

KEGG pathway enrichment analyses were then performed to reveal the functions of these metabolites and their involved signaling pathways. Analyses for positive and negative ion modes were conducted in parallel. Identified metabolic pathways are displayed in Figure 4. In positive ion mode, the top five related pathways were identified as: (1) purine metabolism; (2) aminoacyl-tRNA biosynthesis; (3) valine, leucine and isoleucine biosynthesis; (4) arginine biosynthesis; and (5) nicotinate and nicotinamide metabolism (Figs. 4A, 4B). In negative ion mode, the top five related pathways were identified as: (1) purine metabolism; (2) amine sugar and nucleotide sugar metabolism; (3) galactose metabolism; (4) arginine and proline metabolism; and (5) pyrimidine metabolism (Figs. 4C, D). Interestingly, at P90, untargeted metabolomics confirmed that arginine-related metabolic pathways are altered and enriched among top results in both positive and negative ion modes in *Cep250*$^{-/-}$ mouse retinas (Supplementary Fig. S5). In addition, our results also indicated the main metabolite of arginine-related metabolic pathways, arginine, is upregulated in *Cep250*$^{-/-}$ mice retinas compared to those of WT mice.

Arginase Expression Changes in the Retinas of *Cep250*$^{-/-}$ Mice

Arginase is an enzyme that hydrolyzes arginine to ornithine and urea and which is activated during neuroinflammation. To further validify the suggested arginine dysregulation, we examined arginase expression in the retinas of *Cep250*$^{-/-}$ mice. Arginases are present in two isoforms: arginase 1 (Arg1) and 2 (Arg2). Therefore we examined both ARG1 and ARG2 via immunostaining of mutant and control retinas at P30. Interestingly, immunostaining revealed mislocalization of ARG1 in ONL and lower levels of this protein in the OS of mutants (Fig. 5A), whereas ARG2 did not exhibit notable changes (Fig. 5B). These results suggest that an accumulation of arginine is caused by altered Arg1 expression in *Cep250*$^{-/-}$ mouse retinas.

Investigative Ophthalmology & Visual Science

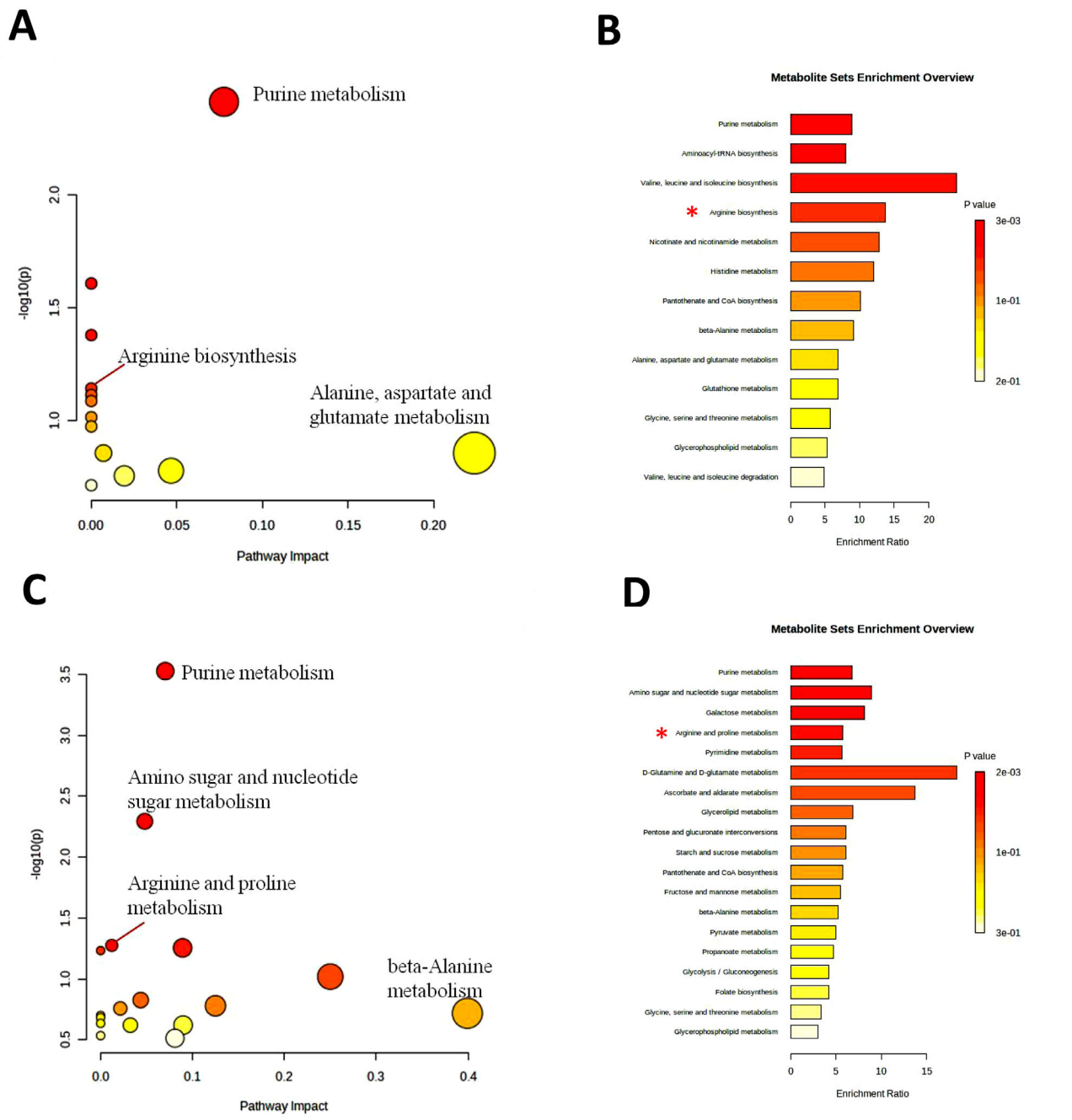

Figure 4. Metabolic pathway and enrichment analysis of differentially expressed metabolites between WT and Cep250 KO mouse retinas at P30. (**A, B**) Pathway analysis and enrichment of differentially expressed metabolites detected in positive ion mode. (**C, D**) Pathway analysis and enrichment of differentially expressed metabolites detected in negative ion mode. Enrichment analysis module conduct metabolite set enrichment analysis based on Kyoto Encyclopedia of Genes and Genomes (KEGG) library. Pathway analysis integrate enrichment analysis and pathway topology analysis. The ratio represents KO/WT. n = 3.

AAV-Based Retinal Arg1 Knockdown Leads to Retinal Degeneration

To further investigate the function of Arg1 in the retina, we used AAV-based subretinal injection to conduct Arg1 knockdown experiments. A schematic representation of these knockdown experiments is displayed in Figure 6A. Subretinal AAV injection was completed at P30, and examinations of retinal functions and structures were performed at P90. To verify AAV expression, fundus photography of AAV-injected retinas was performed at P60. A strong GFP signal was indicative of successful subretinal injection and AAV expression (Fig. 6B). Additionally, the OS ARG1 signal exhibited a reduction in regions with effective AAV infection (Supplementary Fig. S6A). Consistently, elevated levels of arginine were detected in the Arg1-knockdown retinas through quantification using LC-MS/MS (Fig. 6C). OCT results indicated that the thickness of the ONL layer was decreased in

Investigative Ophthalmology & Visual Science

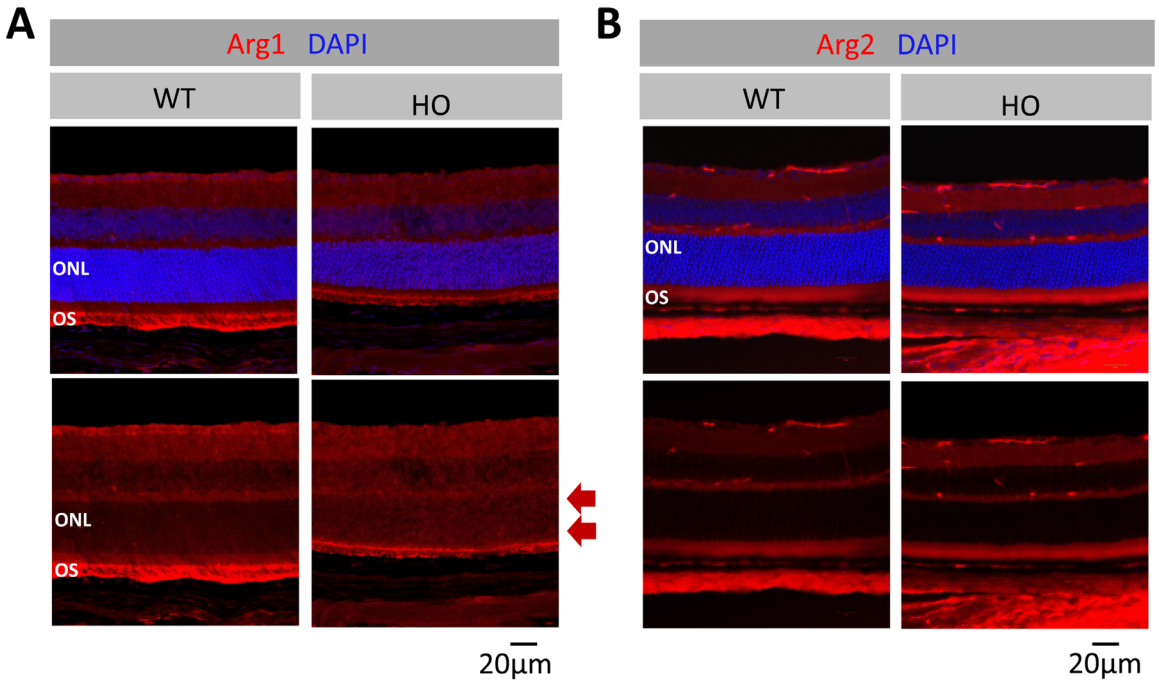

Figure 5. Immunostaining of ARG1 and ARG2 at P30. (**A, B**) Representative images of ARG1 (**A**) and ARG2 (**B**) in Cep250 KO mouse and WT control retinas. *Scale bar*: 20 µm and 50 µm. *Red arrows* indicate the mislocation of ARG1 in the ONL. HO, Homozygotes. n = 3.

Arg1-knockdown retinas (Figs. 6D, 6E). ERG experiments showed significantly lower a-wave and b-wave amplitudes for AAV-Arg1-RNAi WT mouse retinas compared with AAV-Control mice during scotopic ERG responses at two different stimulus intensities (dark 3.0 and dark 10.0; Figs. 6F–I). In addition, we carried out GFAP immunostaining and TUNEL assays to assess retinal degeneration and cell apoptosis, respectively. Interestingly, for these markers of cell degeneration, we observed significant differences between the WT and MT groups (Supplementary Figs. S6B, S6C). Taken together, these results demonstrate photoreceptor degeneration following Arg1 knockdown.

Discussion

Ciliopathy disorders are always characterized by multiorgan involvement, and retinal degeneration is frequently observed.[1–11] Connecting cilia in the photoreceptors act as a pipeline, which is crucial for material transport.[30–33] In cases of ciliary dysfunction, some OS proteins remain permanently stagnate in the cytoplasm, potentially affecting phototransduction functions in multiple mouse models of cilia-related gene mutations.[7–11] However, beyond phototransduction, it remains largely unclear whether the OS compartment plays unidentified functions.[34–38] In our present study, we used untargeted metabolomics and Cep250 KO mice to determine that cilia can transport the metabolic-related protein ARG1 to the OS. Through experiments using an AAV-based knockdown of Arg1, we demonstrated that normal expression of Arg1 is essential for the survival of photoreceptors. These results indicate that the OS may be the compartment for not only phototransduction, but also material metabolism. Nevertheless, it remains to be further investigated whether arginine metabolism has an impact on phototransduction.

Arginase 1 (ARG1) is a key protein in arginine metabolism.[39] It can also modulate immune responses. Arg1-expressing macrophages can inhibit Th2-dependent inflammation through arginine exhaustion, which influences T cell proliferation and stimulation.[40–43] In addition, ARG1 activity decreases the supply of L-arg available for the generation of cytotoxic levels of NO through iNOS.[44–46] Interestingly, recent studies have suggested neuroprotective roles for Arg1 in the retina. Garces et al. found that an increased number of cells expressing the Arg1 marker of neuroprotective microglia in the photoreceptor layer was associated with photoreceptor survival.[47] Mages and colleagues reported that enhanced expression of Arg1 transcripts may indicate improved neuroprotection in the stressed postischemic retina.[48] Furthermore, untargeted metabolic profiling of Norrin KO retinas revealed that arginine and proline metabolism was one of the most enriched upregulated pathways.[49] Another study demonstrated that arginine-related pathways were dysregulated in patients with diabetic retinopathy.[50] Knockout of the other arginase isoform, Arg2, has been suggested to play a protective role against retinal degeneration in an experimental model of autoimmune encephalomyelitis.[51,52] However, the relationship between Arg1 and retinal degeneration remains largely unknown. This study demonstrates, for the first time, that Arg1 knockdown can result in retinal degeneration.

One limitation of our study is that we have not verified whether the CEP250 protein can bind directly to the ARG1 protein. Further work, such as co-IP experiments, will be helpful for better understanding ARG1 transportation. In theory, AAV-based overexpression of the Cep250 gene would reveal more information regarding interactions between CEP250 and ARG1. Unfortunately, the Cep250 transcript is 7977 bp,[53] beyond the maximum capacity of the AAV. Another interesting consideration is whether or not

Investigative Ophthalmology & Visual Science

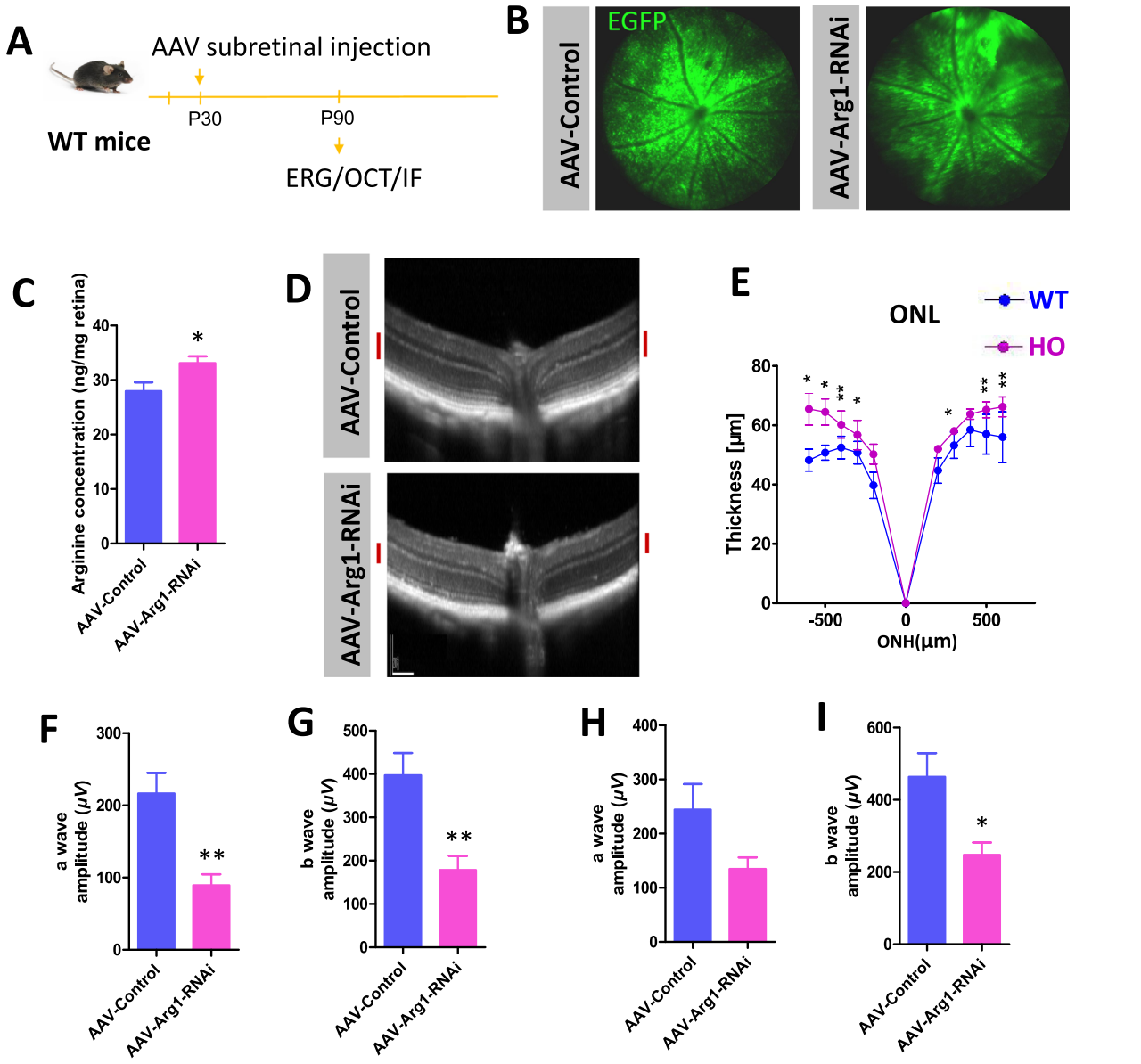

Figure 6. AAV-based retinal Arg1 knockdown experiments in WT mice. (**A**) Schematic representation of knockdown experiments. (**B**) Representative fundus photographs of AAV-injected retinas at P60. Strong GFP signals were indicative of successful subretinal injection and AAV expression. (**C**) Retinal arginine quantification of the AAV injected mouse retinas. (**D**) The *short red lines* on the right sides of the OCT images indicate that ONL layer thickness was decreased in the retinas of Arg1 knockdown mice. *Scale bar*: 100 µm. (**E**) Measurements of the thicknesses of the ONL from OCT images of mice at P90. ONH, optic nerve head. Normalized values represent mean ± SEM.*P < 0.05, and **P < 0.01, Student's t test. n = 5. (**F–I**) Statistical analysis of a-wave and b-wave amplitudes at dark 3.0 (**F, G**) and dark 10.0 (**H, I**) in WT mice injected with AAV-Control and AAV-Arg1-RNAi.

the interaction between CEP250 and ARG1 is specific. In other words, can ARG1 interact with other cilia-related proteins? Indeed, we could cross an Arg1 KO mouse line with a Cep250 KO mouse line to make it more likely to observe faster or more serious phenotypic retinal changes. Although a previously published article reported that the OCT layers of the heterozygous Arg1 KO mice look normal,[54] we cannot rule out the potential occurrence of degeneration in long-term follow-up studies, especially in homozygotes.

In addition to arginine-related metabolic pathways, we noted that pathways related to nicotinate and nicotinamide metabolism were significantly altered in the retinas of Cep250 KO mice at P30 and P90. Thus we cannot exclude the potential important roles of other pathways beyond arginine-related pathways. These unidentified metabolic changes may also affect the degeneration processes in KO mice. Moreover, both arginine and proline metabolism, as well as arginine biosynthesis, may contribute to the accumulation of arginine in Cep250 KO mice. These findings are intriguing and warrant further investigation in future studies. In our present study, we found that dysregulated arginine metabolism plays an essential role in retinal degeneration in Cep250 KO mice. Our findings provide novel insights and increase our understanding of retinal degeneration in ciliopathy disorders.

Investigative Ophthalmology & Visual Science

Acknowledgments

Supported by grants from the National Natural Science Foundation of China (81800857), the Zhejiang Provincial Natural Science Foundation of China (LY23H120015, LTGD23H120001, LGD22H120001, LTGC23H120001).

Disclosure: **L. Xiang,** None; **Q-L. Yang,** None; **B-T. Xie,** None; **H-Y. Zeng,** None; **L-J. Ding,** None; **F-Q. Rao,** None; **T. Yan,** None; **F. Lu,** None; **Q. Chen,** None; **X-F. Huang,** None

References

1. Chandra B, Tung ML, Hsu Y, Scheetz T, Sheffield VC. Retinal ciliopathies through the lens of Bardet-Biedl Syndrome: past, present and future. *Progr Retinal Eye Res*. 2022;89:101035.
2. Reiter JF, Leroux MR. Genes and molecular pathways underpinning ciliopathies. *Nat Rev Mol Cell Biol*. 2017;18:533–547.
3. Baehr W, Hanke-Gogokhia C, Sharif A, et al. Insights into photoreceptor ciliogenesis revealed by animal models. *Progress in Retinal and Eye Research*. 2019;71:26–56.
4. Downs LM, Scott EM, Cideciyan AV, et al. Overlap of abnormal photoreceptor development and progressive degeneration in Leber congenital amaurosis caused by NPHP5 mutation. *Hum Mol Genet*. 2016;25:4211–4226.
5. Rannar Airik, Slaats Gisela G, Guo Zhi, et al. Renal-retinal ciliopathy gene Sdccag8 regulates DNA damage response signaling. *J Am Soc Nephrol*. 2014;25:2573–2583.
6. Slaats Gisela G, Ghosh Amiya K, Falke Lucas L, et al. Nephronophthisis-associated CEP164 regulates cell cycle progression, apoptosis and epithelial-to-mesenchymal transition. *PLoS Genet*. 2014;10:e1004594.
7. Ronquillo CC, Hanke-Gogokhia C, Revelo MP, Frederick JM, Jiang L, Baehr W. Ciliopathy-associated IQCB1/NPHP5 protein is required for mouse photoreceptor outer segment formation. *FASEB J*. 2016;30:3400–3412.
8. Sharif AS, Gerstner CD, Cady MA, et al. Deletion of the phosphatase INPP5E in the murine retina impairs photoreceptor axoneme formation and prevents disc morphogenesis. *J Biol Chem*. 2021;296:100529.
9. Guo D, Ru J, Xie L, et al. Tmem138 is localized to the connecting cilium essential for rhodopsin localization and outer segment biogenesis. *Proc Natl Acad Sci USA*. 2022;119(15):e2109934119.
10. Dilan TL, Moye AR, Salido EM, et al. ARL13B, a Joubert syndrome–associated protein, is critical for retinogenesis and elaboration of mouse photoreceptor outer segments. *J Neurosci*. 2019;39:1347–1364.
11. Mookherjee S, Chen HY, Isgrig K, et al. A CEP290 C-Terminal domain complements the mutant CEP290 of Rd16 mice in trans and rescues retinal degeneration. *Cell Reports*. 2018;25:611–623.
12. Cheng SY, Cipi J, Ma S, et al. Altered photoreceptor metabolism in mouse causes late stage age-related macular degeneration-like pathologies. *Proc Natl Acad Sci USA*. 2020;117:13094–13104.
13. Grenell A, Wang Y, Yam M, et al. Loss of MPC1 reprograms retinal metabolism to impair visual function. *Proc Natl Acad Sci USA*. 2019;116:3530–3535.
14. Sasaki Y, Kakita H, Kubota S, et al. SARM1 depletion rescues NMNAT1-dependent photoreceptor cell death and retinal degeneration. *eLife*. 2020;9:e62027.
15. Sinha T, Du J, Makia MS, Hurley JB, Naash MI, Al-Ubaidi MR. Absence of retbindin blocks glycolytic flux, disrupts metabolic homeostasis, and leads to photoreceptor degeneration. *Proc Natl Acad Sci USA*. 2021;118(6):e2018956118.
16. Xiang L, Chen XJ, Wu KC, et al. miR-183/96 plays a pivotal regulatory role in mouse photoreceptor maturation and maintenance. *Proc Natl Acad Sci USA*. 2017;114:6376–6381.
17. Xu L, Kong L, Wang J, Ash JD. Stimulation of AMPK prevents degeneration of photoreceptors and the retinal pigment epithelium. *Proc Natl Acad Sci USA*. 2018;115:10475–10480.
18. Masek M, Etard C, Hofmann C, et al. Loss of the Bardet-Biedl protein Bbs1 alters photoreceptor outer segment protein and lipid composition. *Nat Commun*. 2022;13(1):1282.
19. Do Rhee K, Wang Y, ten Hoeve J, et al. Ciliary neurotrophic factor-mediated neuroprotection involves enhanced glycolysis and anabolism in degenerating mouse retinas. *Nat Commun*. 2022;13(1):7037.
20. Lains I, Mendez K, Nigalye A, et al. Plasma metabolomic profiles associated with three-year progression of age-related macular degeneration. *Metabolites*. 2022;12(1):32.
21. Wang Z, Tang J, Jin E, et al. Serum untargeted metabolomics reveal potential biomarkers of progression of diabetic retinopathy in Asians. *Front Mol Biosci*. 2022;9:871291.
22. Zhou Y, Xu Y, Zhang X, et al. Plasma metabolites in treatment-requiring retinopathy of prematurity: potential biomarkers identified by metabolomics. *Exp Eye Res*. 2020;199:108198.
23. Weiss ER, Osawa S, Xiong Y, et al. Broad spectrum metabolomics for detection of abnormal metabolic pathways in a mouse model for retinitis pigmentosa. *Exp Eye Res*. 2019;184:135–145.
24. Hou XW, Wang Y, Ke CF, Li MY, Pan CW. Metabolomics and biomarkers in retinal and choroidal vascular diseases. *Metabolites*. 2022;12:814.
25. Laíns I, Gantner M, Murinello S, et al. Metabolomics in the study of retinal health and disease. *Prog Retin Eye Res*. 2019;69:57–79.
26. Zhang CJ, Xiang L, Chen XJ, et al. Ablation of mature miR-183 leads to retinal dysfunction in mice. *Invest Ophthalmol Vis Sci*. 2020;61(3):12.
27. Zhuang YY, Xiang L, Wen XR, et al. Slc7a14 Is indispensable in zebrafish retinas. *Front Cell Dev Biol*. 2019;7:333.
28. Xiang L, Zhang J, Rao FQ, et al. Depletion of miR-96 delays, but does not arrest, photoreceptor development in mice. *Invest Ophthalmol Vis Sci*. 2022;63(4):24.
29. Santucci L, Lomuscio S, Primiano A, et al. Development of a novel ultra performance liquid chromatography tandem-mass spectrometry (UPLC-MS/MS) method to measure l-arginine metabolites in plasma. *Clin Chim Acta*. 2023;543:117306.
30. Mercey O, Kostic C, Bertiaux E, et al. The connecting cilium inner scaffold provides a structural foundation that protects against retinal degeneration. *PLoS Biol*. 2022;20(6):e3001649.
31. Boldt K, Mans DA, Won J, et al. Disruption of intraflagellar protein transport in photoreceptor cilia causes Leber congenital amaurosis in humans and mice. *J Clin Invest*. 2011;121:2169–2180.
32. Gotthardt K, Lokaj M, Koerner C, Falk N, Giessl A, Wittinghofer A. A G-protein activation cascade from Arl13B to Arl3 and implications for ciliary targeting of lipidated proteins. *eLife*. 2015;4:e11859.
33. Hsu YC, Chuang JZ, Sung CH. Light regulates the ciliary protein transport and outer segment disc renewal of mammalian photoreceptors. *Dev Cell*. 2015;32(6):731–742.
34. Pearring JN, Martínez-Márquez J, Willer JR, Lieu EC, Salinas RY, Arshavsky VY. The GARP domain of the rod CNG channel's β1-subunit contains distinct sites for outer segment targeting and connecting to the photoreceptor disk rim. *J Neurosci*. 2021;41:3094–3104.

35. Fang X, Peden AA, van Eeden FJM, Malicki JJ. Identification of additional outer segment targeting signals in zebrafish rod opsin. *J Cell Sci*. 2021;134(6):jcs254995.
36. Pearring JN, Salinas RY, Baker SA, Arshavsky VY. Protein sorting, targeting and trafficking in photoreceptor cells. *Prog Retin Eye Res*. 2013;36:24–51.
37. Vinberg F, Chen J, Kefalov VJ. Regulation of calcium homeostasis in the outer segments of rod and cone photoreceptors. *Prog Retin Eye Res*. 2018;67:87–101.
38. Peshenko IV, Olshevskaya EV, Dizhoor AM. Retinal degeneration-3 protein attenuates photoreceptor degeneration in transgenic mice expressing dominant mutation of human retinal guanylyl cyclase. *J Biol Chem*. 2021;297(4):101201.
39. Hannemann N, Cao S, Eriksson D, et al. Transcription factor Fra-1 targets arginase-1 to enhance macrophage-mediated inflammation in arthritis. *J Clin Invest*. 2019;129:2669–2684.
40. Pesce JT, Ramalingam TR, Mentink-Kane MM, et al. Arginase-1–expressing macrophages suppress Th2 cytokine–driven inflammation and fibrosis. *PLoS Pathog*. 2009;5(4):e1000371.
41. Monin L, Griffiths KL, Lam WY, et al. Helminth-induced arginase-1 exacerbates lung inflammation and disease severity in tuberculosis. *J Clin Invest*. 2015;125:4699–4713.
42. Mondanelli G, Ugel S, Grohmann U, Bronte V. The immune regulation in cancer by the amino acid metabolizing enzymes ARG and IDO. *Curr Opin Pharmacol*. 2017;35:30–39.
43. Munder M, Choi BS, Rogers M, Kropf P. L-Arginine deprivation impairs *Leishmania major*–specific T-cell responses: immunity to infection. *Eur J Immunol*. 2009;39(8):2161–2172.
44. Kropf P, Fuentes JM, Fähnrich E, et al. Arginase and polyamine synthesis are key factors in the regulation of experimental leishmaniasis in vivo. *FASEB J*. 2005;19:1000–1002.
45. Rutschman R, Lang R, Hesse M, Ihle JN, Wynn TA, Murray PJ. Cutting edge: stat6-dependent substrate depletion regulates nitric oxide production. *J Immunol*. 2001;166:2173–2177.
46. Schleicher U, Paduch K, Debus A, et al. TNF-mediated restriction of arginase 1 expression in myeloid cells triggers type 2 NO synthase activity at the site of infection. *Cell Rep*. 2016;15:1062–1075.
47. Garces K, Carmy T, Illiano P, Brambilla R, Hackam AS. Increased neuroprotective microglia and photoreceptor survival in the retina from a peptide inhibitor of myeloid differentiation factor 88 (MyD88). *J Mol Neurosci*. 2020;70(6):968–980.
48. Mages K, Grassmann F, Jägle H, et al. The agonistic TSPO ligand XBD173 attenuates the glial response thereby protecting inner retinal neurons in a murine model of retinal ischemia. *J Neuroinflammation*. 2019;16:43.
49. Heng JS, Rattner A, Stein-O'Brien GL, et al. Hypoxia tolerance in the Norrin-deficient retina and the chronically hypoxic brain studied at single-cell resolution. *Proc Natl Acad Sci USA*. 2019;116:9103–9114.
50. Sumarriva K, Uppal K, Ma C, et al. Arginine and carnitine metabolites are altered in diabetic retinopathy. *Invest Ophthalmol Vis Sci*. 2019;60:3119.
51. Palani CD, Fouda AY, Liu F, et al. Deletion of arginase 2 ameliorates retinal neurodegeneration in a mouse model of multiple sclerosis. *Mol Neurobiol*. 2019;56:8589–8602.
52. Candadai AA, Liu F, Fouda AY, et al. Deletion of arginase 2 attenuates neuroinflammation in an experimental model of optic neuritis. *Plos One*. 2021;16(3):e0247901.
53. Huang X, Xiang L, Fang X, et al. Functional characterization of *CEP250* variant identified in nonsyndromic retinitis pigmentosa. *Hum Mutat*. 2019;40:1039–1045.
54. Fouda AY, Xu Z, Shosha E, et al. Arginase 1 promotes retinal neurovascular protection from ischemia through suppression of macrophage inflammatory responses. *Cell Death Dis*. 2018;9:1001.